THE JOURNAL OF BIOLOGICAL CHEMISTRY VOL. 282, NO. 12, pp. 9162–9171, March 23, 2007

Tryptophan-scanning Mutagenesis in the αM3 Transmembrane Domain of the Muscle-type Acetylcholine Receptor

*A SPRING MODEL REVEALED**

Received for publication, August 7, 2006, and in revised form, January 18, 2007 Published, JBC Papers in Press, January 22, 2007, DOI 10.1074/jbc.M607492200

José David Otero-Cruz[‡], Carlos Alberto Báez-Pagán[‡], Iván Manuel Caraballo-González[§], and José Antonio Lasalde-Dominicci[§1]

From the Departments of [‡]Chemistry and [§]Biology, University of Puerto Rico, Río Piedras Campus, San Juan P. R. 00931, Puerto Rico

Membrane proteins constitute a large fraction of all proteins, yet very little is known about their structure and conformational transitions. A fundamental question that remains obscure is how protein domains that are in direct contact with the membrane lipids move during the conformational change of the membrane protein. Important structural and functional information of several lipid-exposed transmembrane domains of the acetylcholine receptor (AChR) and other ion channel membrane proteins have been provided by the tryptophan-scanning mutagenesis. Here, we use the tryptophan-scanning mutagenesis to monitor the conformational change of the αM3 domain of the muscle-type AChR. The perturbation produced by the systematic tryptophan substitution along the αM3 domain were characterized through two-electrode voltage clamp and ^{125}I-labeled α-bungarotoxin binding. The periodicity profiles of the changes in AChR expression (closed state) and ACh EC_{50} (open-channel state) disclose two different helical structures; a thinner-elongated helix for the closed state and a thicker-shrunken helix for the open-channel state. The existence of two different helical structures suggest that the conformational transition of the αM3 domain between both states resembles a spring motion and reveals that the lipid-AChR interface plays a key role in the propagation of the conformational wave evoked by agonist binding. In addition, the present study also provides evidence about functional and structural differences between the αM3 domains of the *Torpedo* and muscle-type receptors AChR.

The acetylcholine receptor (AChR)[2] belongs to the superfamily of the ligand-gated ion channel receptors that are of fundamental importance in the chemical synaptic transmission throughout the nervous system (1–4). Defects in the AChR function could affect the transmission of nerve signals across synapses and cause pathological diseases such as the congenital myasthenic syndromes (5). The AChR is composed of five homologous membrane-spanning subunits, $2\alpha_1\beta_1\delta\epsilon$, assembled quasi-pentamerically around a central axis, forming a cation-selective ion channel (6). Each subunit contains a large hydrophilic extracellular N terminus, 4 putative transmembrane domains of 19–25 amino acids denoted as M1–M4, a large cytoplasmic loop between the M3 and M4 domains, and a short extracellular C terminus (7). The M1 and M2 domains form the ion channel pore (8, 9), whereas the M3 and M4 domains form the outer contour, having the largest contact with the lipid membrane (10), and are distant from the ion channel pore and from the ligand binding sites (6).

Different experimental approaches have revealed dynamic information about agonist-induced conformational changes of the pore forming domains (M1 and M2) (8, 11–14). It is noteworthy that a recent study suggested that there is no significant movement of the pore lining domains during channel activation of the AChR (14). However, a previous study found significant structural differences in the membrane domains of the AChR channel lumen among resting, open, and desensitized states (11). A great deal of information about the conformational changes of the ion pore-forming domains of the AChR has been obtained from single channel kinetics, which have been mainly obtained from studies in the muscle-type AChR (15, 16). Until now, a high resolution structure of the AChR remains elusive; however, the *Torpedo marmorata* AChR structure from cryoelectron microscopic images (6) has been widely used as a model to establish structure-function relationships of the muscle-type AChR data. Along this line, the structural and functional differences in the transmembrane domains between the *Torpedo* and muscle-type AChRs remain to be established.

The lipid-exposed transmembrane domains (M3 and M4) have been implicated in the dynamics of the AChR (17–37); however, it remains unclear how these domains move during the acetylcholine (ACh)-induced activation and their contribution to the AChR gating. A list of photolabeling affinity studies has clearly demonstrated that there is a large change in the degree of lipid contact of the lipid-exposed transmembrane domains between the resting and agonist-induced desensitized

* This work was supported in part by National Institutes of Health Grants 2RO1GM56371-09 and GM08102-27 and University of Puerto Rico Institutional Funds for Research (to J. A. L.-D.), National Institutes of Health-Minority Biomedical Research Support Research Initiative for Scientific Enhancement Grant R25GM61151 (to C. A. B.-P. and J. D. O.-C.), and the National Science Foundation Alliance for Graduate Education and the Professoriate HRD-0302696 (to C. A. B.-P. and J. D. O.-C.). The costs of publication of this article were defrayed in part by the payment of page charges. This article must therefore be hereby marked "*advertisement*" in accordance with 18 U.S.C. Section 1734 solely to indicate this fact.

[1] To whom correspondence should be addressed to. Tel.: 787-764-0000 (ext. 1-2765 or 4887); Fax: 787-753-3852; E-mail: joseal@coqui.net or jlasalde@gmail.com.

[2] The abbreviations used are: AChR, acetylcholine (ACh) receptor; BgTx, bungarotoxin; TrpScanM, tryptophan-scanning mutagenesis; WT, wild type.

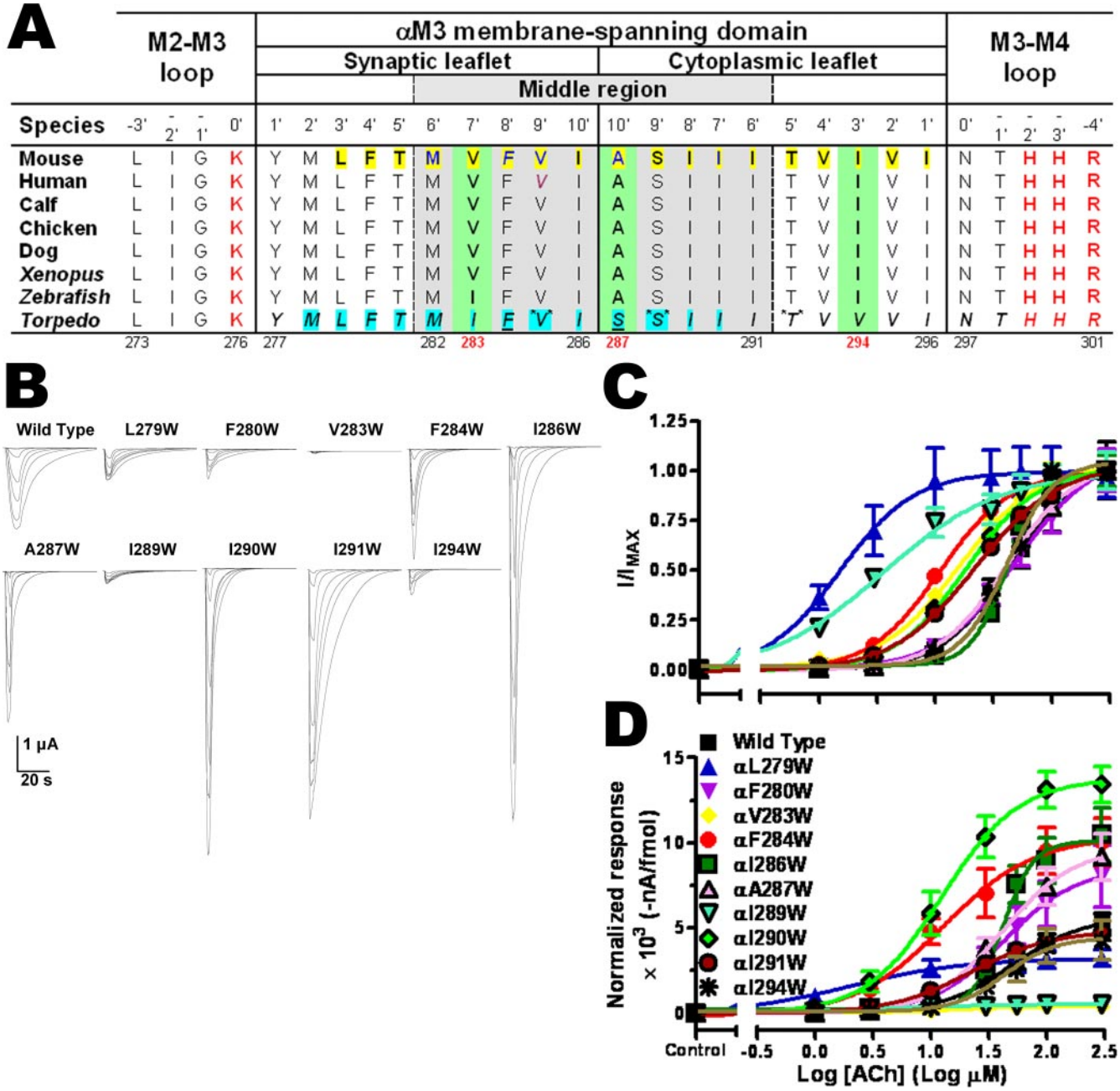

FIGURE 1. **Sequence alignments of the αM3 domain and functional response of wild type and αM3-mutant AChRs.** *A*, LFTMV*F*VIASIIITVIVI (highlighted in *yellow*) were examined in the current study. MFVAI (*blue font*) and *MLFTMIF**V*I*S***S***II* (highlighted in *turquoise*) were studied using tryptophan-scanning mutagenesis and patch clamp (32). *V* (*violet font* and *italic*) and *F* (*blue font* and *italic*) were studied using site-directed mutagenesis and patch clamp (23, 31). *F* and *S* were labeled as lipid-exposed using photolabeling affinity (10). *YMLFTMIF**V*I*S***S***III***T***VVVINTHHR* (*italic*) were studied using NMR spectroscopy (79). **V**, **S**, and **T** were revealed as residues that form stable hydrogen bonds among them using NMR spectroscopy (79). KHHR (*red font*) are basic amino acids. V283I, A287S, and I294V are non-conserved residues. The *numbers* at the *bottom* indicate the position in the mouse skeletal muscle α_1-subunit. *B* shows representative families of macroscopic ionic current traces evoked by 1–300 μM ACh and recorded through voltage clamp. *C* and *D* display dose-response curves that were standardized to ^{125}I-labeled α-bungarotoxin (fmol) bound to AChR expressed on the oocyte surface membrane (*C*) and that were normalized to maximum ionic current (*D*).

states, therefore suggesting that these domains display a substantial conformational change upon agonist-induced activation of the AChR (10, 12, 13, 38, 39). A recent study reported structural and conformational changes in the third transmembrane domain of a homologous receptor, the αM3 domain of the γ-aminobutyric acid type A receptor (40). In the present study we used the tryptophan-scanning mutagenesis (Trp-ScanM) approach to monitor the conformational changes experienced by the muscle-type AChR αM3 domain (Fig. 1*A*). This approach has been used successfully for inward rectifier potassium channels (41–43), voltage-activated potassium channels (44–50), nicotinic AChR channels (25, 32, 34, 35), glutamate receptor channels (51), γ-aminobutyric acid type A receptor channels (52, 53), voltage-gated sodium channels (54), *N*-methyl-D-aspartate receptor channels (55), $P2X_4$ receptor channels (56), mechanosensitive channels MscL (57), human

ether-a-go-go-related gene (HERG) K^+ channels (58), and epithelial Na^+ channels (59). The present TrpScanM approach allowed us to construct structural models of the muscle-type AChR αM3 domain in both the closed- and open-channel states and to compare between *Torpedo* and muscle-type AChRs. The interpretation of these structural models led us to postulate a spring model. The spring model proposes that channel gating could be linked to the helical structure stability of the lipid-exposed transmembrane domains in the open-channel state. Further examination of the spring model in other ion channels will open new avenues that could potentially increase our understanding on how lipid-exposed domains regulate ion channel function in general. Finally, the comparison of the TrpScanM data between the αM3 domain of the muscle-type and *Torpedo* AChRs also reveals localized conformational differences that could contribute to the functional differences between these receptors.

EXPERIMENTAL PROCEDURES

General Experimental Procedures—Xenopus laevis oocytes were microinjected with the mouse muscle adult-type AChR complementary RNAs (see also Refs. 25, 32, 34, and 35). Mutations were engineered with the QuikChange® site-directed mutagenesis kit (Stratagene) and were confirmed by automated DNA sequencing. All mutagenic primers were designed with the tryptophan codon (TGG) instead of the wild type (WT) codon at the desired position. Muscle-type AChR cRNA transcripts were synthesized with the mMESSAGE mMACHINE® kit (Ambion). Oocytes were incubated for 3–5 days with fresh liquid medium at 19 °C.

Voltage Clamp—Macroscopic ACh-induced currents were recorded with a whole-cell two-electrode voltage clamp configuration using the Gene Clamp 500B amplifier (Axon Instruments) at room temperature. Electrodes were filled with 3 M KCl, resistances were <2 megaohms. Impaled oocytes were automatically perfused with MOR-2 buffer (82.5 mM NaCl, 2.5 mM KCl, 5 mM $MgCl_2$, 1 mM Na_2HPO_4, 0.2 mM $CaCl_2$, 5 mM HEPES, and 0.5 mM EGTA (pH 7.4)) at a rate of 0.43 ml/s using a Perfusion Valve Controller VC-8 (Warner Instruments). Membrane potential was held at −70 mV. Membrane currents were filtered at 100 Hz and digitized at 1 kHz using a DigiData 1322A interface (Axon Instruments). Data acquisition was conducted through the Clampex 9.2 program (Axon Instruments). Dose-response curves were generated from macroscopic peak currents (I) obtained from 7 different ACh concentrations (1, 3, 10, 30, 55, 100, and 300 μM ACh). Dose-response curves were fitted through the sigmoidal dose-response equation with variable slope using the GraphPad Prism 4 program (GraphPad),

$$I(\text{nA}) = I_{\text{min}} + \frac{I_{\text{max}} - I_{\text{min}}}{1 + 10^{(\log EC_{50} - \log[\text{ACh}]) \times \text{Hill slope}}} \qquad \text{(Eq. 1)}$$

where I is the macroscopic peak ionic current at a given ACh concentration, I_{min} and I_{max} are the smallest and the largest currents observed, respectively, EC_{50} is the concentration of acetylcholine that provokes a response halfway between I_{min} and I_{max}, and the Hill slope is the steepness of the dose-response curve.

^{125}I-Labeled α-Bungarotoxin Binding Assays—^{125}I-Labeled α-bungarotoxin (^{125}I-labeled α-BgTx) (PerkinElmer Life Sciences) binding assays were performed immediately after the voltage clamp measurement for the same intact oocytes. Oocytes were incubated in 20 nM ^{125}I-labeled α-BgTx, 5 mg/ml bovine serum albumin, MOR-2 without EGTA, and in the absence of agonist at room temperature for 2 h. Non-injected oocytes were incubated under the same conditions to measure nonspecific binding. The excess of toxin was removed by washing each oocyte with 25 ml of MOR-2 without EGTA. Calibration curves were plotted with radioactivity (counts/min) as a function of concentration ^{125}I-labeled α-BgTx (fmol). Calibration curves were used to determine the AChR expression levels in each oocyte. Radioactivity was measured using a Beckman 5500 γ counter (Beckman Coulter).

Normalized Macroscopic AChR Response—The normalized response (nA/fmol) of each oocyte was assessed as the ratio of the macroscopic peak current (nA) generated at 300 μM ACh to the superficial ^{125}I-labeled α-BgTx binding (fmol).

Statistical Analysis—Each αM3-mutant was compared against the WT for each parameter using a one-way analysis of variance with Dunnett's post-test performed in the GraphPad Prism 4 program (see Table 1). The mean of the number of residues per turn of the closed- and open-channel states was compared using an unpaired t test with Welch's correction through the GraphPad Prism 4 program.

Periodicity Profiles—The number of residues per helical turn for the closed- and open-channel states was determined by the AChR expression and ACh EC_{50} periodicity profiles, respectively (see Fig. 2, *A–D*). The AChR expression of each mutant was standardized to the change in amino acid volume (Å^3) caused by each tryptophan substitution (fmol/Å^3). Standardized expression ($X_{\text{standardized}}$) was calculated as,

$$X_{\text{standardized}}\ (\text{fmol/Å}^3) = \frac{X_{\text{mutant}}}{V_{\text{Trp}} - V_{\text{WT}}} \qquad \text{(Eq. 2)}$$

where X_{mutant} is the expression of the αM3 mutant AChRs, and V_{Trp} and V_{WT} are the volumes of the tryptophan and original residues, respectively. Amino acid volume values (V_{Trp} and V_{WT}) are from crystallographic studies (60). Periodicity profiles were plotted with ACh EC_{50} or AChR expression as function of their tryptophan substitution position along the αM3 domain. Periodicity curves were created through the cubic spline method with 3000 segments using the GraphPad Prism 4 program. The number of residues per helical turn of the periodicity profiles was estimated as the number of amino acids between the adjacent maximums and minimums peaks.

Helical Net Diagrams—Helical net diagrams were built using the number of residues between the adjacent maximum and minimum peaks of the periodicity profile for the open-channel state (see Fig. 2*D*). Rotation angle (Ω) per residue for each helical turn was calculated as,

$$\Omega(\text{degree}) = \frac{360°}{n} \qquad \text{(Eq. 3)}$$

where n is the number of residues per helical turn. Helical rise per residue (d) for each helical turn was determined using,

TABLE 1

Biophysical parameters of the wild type and αM3-mutant AChRs

Values are given as the mean ± S.E. for each parameter and was calculated using 15–27 oocytes. ND means no detectable current.

AChR type	Expression level	EC_{50}	Hill coefficient	I_{max}	Normalized response[a]
	fmol	μM		*−nA*	*−nA/fmol*
$2\alpha_1\beta_1\delta\epsilon$ (wild type)	0.33 ± 0.02	46 ± 2	1.5 ± 0.5	2402 ± 288	5649 ± 625
$2\alpha_1$(L279W)$\beta_1\delta\epsilon$	0.5 ± 0.1	3 ± 1[c]	1.4 ± 0.6	855 ± 53[c]	3374 ± 367[c]
$2\alpha_1$(F280W)$\beta_1\delta\epsilon$	0.12 ± 0.03	50 ± 2[b]	1.3 ± 0.3	743 ± 82[c]	8514 ± 1526[c]
$2\alpha_1$(T281W)$\beta_1\delta\epsilon$	0.4 ± 0.1	ND	ND	ND	ND
$2\alpha_1$(M282W)$\beta_1\delta\epsilon$	0.24 ± 0.02	ND	ND	ND	ND
$2\alpha_1$(V283W)$\beta_1\delta\epsilon$	0.26 ± 0.06	16 ± 1[c]	1.3 ± 0.2	61 ± 3[c]	406 ± 36[c]
$2\alpha_1$(F284W)$\beta_1\delta\epsilon$	0.20 ± 0.01	10 ± 1[c]	1.0 ± 0.6	2923 ± 276[c]	10046 ± 536[c]
$2\alpha_1$(V285W)$\beta_1\delta\epsilon$	0.13 ± 0.02	ND	ND	ND	ND
$2\alpha_1$(I286W)$\beta_1\delta\epsilon$	1.1 ± 0.2[c]	41 ± 1[c]	2.7 ± 0.5[c]	9190 ± 427[c]	10084 ± 735[c]
$2\alpha_1$(A287W)$\beta_1\delta\epsilon$	0.30 ± 0.03	37 ± 1[c]	1.4 ± 0.6	4005 ± 345[c]	9178 ± 490[c]
$2\alpha_1$(S288W)$\beta_1\delta\epsilon$	0.1 ± 0.2	ND	ND	ND	ND
$2\alpha_1$(I289W)$\beta_1\delta\epsilon$	0.66 ± 0.09[c]	4 ± 1[c]	0.9 ± 0.2	310 ± 21[c]	538 ± 36[c]
$2\alpha_1$(I290W)$\beta_1\delta\epsilon$	0.34 ± 0.01	16 ± 1[c]	1.4 ± 0.6	6692 ± 174[c]	13418 ± 276[c]
$2\alpha_1$(I291W)$\beta_1\delta\epsilon$	1.28 ± 0.09[c]	22 ± 1[c]	1.2 ± 0.1	6093 ± 195[c]	4847 ± 189[b]
$2\alpha_1$(T292W)$\beta_1\delta\epsilon$	0.08 ± 0.03	ND	ND	ND	ND
$2\alpha_1$(V293W)$\beta_1\delta\epsilon$	0.05 ± 0.04[b]	ND	ND	ND	ND
$2\alpha_1$(I294W)$\beta_1\delta\epsilon$	0.07 ± 0.04[b]	42 ± 1[b]	2 ± 1	558 ± 68[c]	4444 ± 735[c]
$2\alpha_1$(V295W)$\beta_1\delta\epsilon$	0.21 ± 0.05	ND	ND	ND	ND
$2\alpha_1$(I296W)$\beta_1\delta\epsilon$	0.29 ± 0.04	ND	ND	ND	ND

[a] The normalized response (nA/fmol) of each oocyte was assessed as the ratio of the macroscopic peak current (nA) generated at 300 μM ACh to the superficial ^{125}I-labeled α-BgTx binding (fmol).
[b] $0.01 \leq p < 0.05$.
[c] $0.001 \leq p < 0.01$.

$$d(\text{Å}) = \frac{p}{n} \times \Delta + b \qquad \text{(Eq. 4)}$$

where Δ is the number of amino acids between the positions of the residue and anterior peak, b is the magnitude of the maximum rise in the anterior helical turn (thus, the rise at 360°), and the helical pitch (p) per helical turn was estimated through p (Å) $= -1 \times n + 9$ (n is the number of residues per helical turn).

Molecular Modeling—The structural models of the closed- and open-channel states were built with the periodicity profile data using the Deep Viewer/Swiss-PdbViewer 3.7 program (Swiss-Pdb Viewer). The backbone of each helical structure was adjusted to the number of residues per helical turn determined by periodicity profiles using,

$$3\cos\Omega = 1 - 4\cos^2\left(\frac{\varphi + \psi}{2}\right) \qquad \text{(Eq. 5)}$$

where Ω is rotation angle per residue, and φ and ψ are backbone dihedral angles. The helical structures were energetically minimized. The backbones of the helical structures were superimposed to compare their structure. The quality of the superimposition between two helical structures was evaluated by calculating the root mean squared deviation. The mobility of the backbone atoms between helical structures was displayed using B-factor in the superposed models. The length (h), helical pitch (p), and helical rise per amino acid (d) of the helical structure were calculated through the Deep Viewer/Swiss-Pdb-Viewer 3.7 program. The radio (r) of the helical structure was estimated using $r^2 = (p/2)^2 + d^2$, considering the helical structure as a cylinder. The volume (V) of the helical structure was assessed using $V = \pi r^2 h$. Molecular graphics generated in the Swiss-PdbViewer program were exported to the PyMOL™ Molecular Graphics System program (DeLano Scientific LLC) (see Fig. 3) to produce images of the highest quality.

RESULTS

Functional Characterization of the αM3 Mutations—All the αM3 mutants showed different AChR expression levels (Table 1). Two of the αM3 mutations (V293W and I294W) displayed a significant reduction in the AChR expression levels compared with WT. Although the other four mutations displayed an apparent reduction in AChR expression levels (*i.e.* F280W, V285W, S288W, and T292W), a detailed statistical analysis shown in Table 1 suggests that the expression of these mutants is not significantly different from WT. The other three mutations (I286W, I289W, and I291W) showed 200–400% higher AChR expression levels compared with WT, suggesting a facilitation of oligomerization and/or assembly induced by these mutations. The remaining nine mutations (L279W, T281W, M282W, V283W, F284W, A287W, I290W, V295W, and I296W) exhibited similar AChR expression levels as WT. These expression results have demonstrated that a bulky side chain can be accommodated along the αM3 transmembrane domain of the muscle-type AChR, although eight mutations (T281W, M282W, V285W, S288W, T292W, V293W, V295W, and I296W) were incapable of eliciting ACh-induced currents (Fig. 1*B* and Table 1). This loss of ion channel function in the aforementioned mutations could be a consequence of the steric hindrance introduced by the bulky tryptophan side chain.

All the mutations that produced functional AChRs showed a typical sigmoidal ACh dose-response curve except I286W and I289W, which exhibited steeper and shallower curve profiles, respectively (Fig. 1*C*). The dose-response behavior of I286W and I289W suggests a notable change in the allosteric properties of the AChR. Four mutations (I286W, A287W, I290W, and I291W) enhanced the maximum macroscopic response by 150–400% compared with WT (Table 1). The remaining six mutations (L279W, F280W, V283W, F284W, I289W, and I294W) significantly reduced the maximum macroscopic

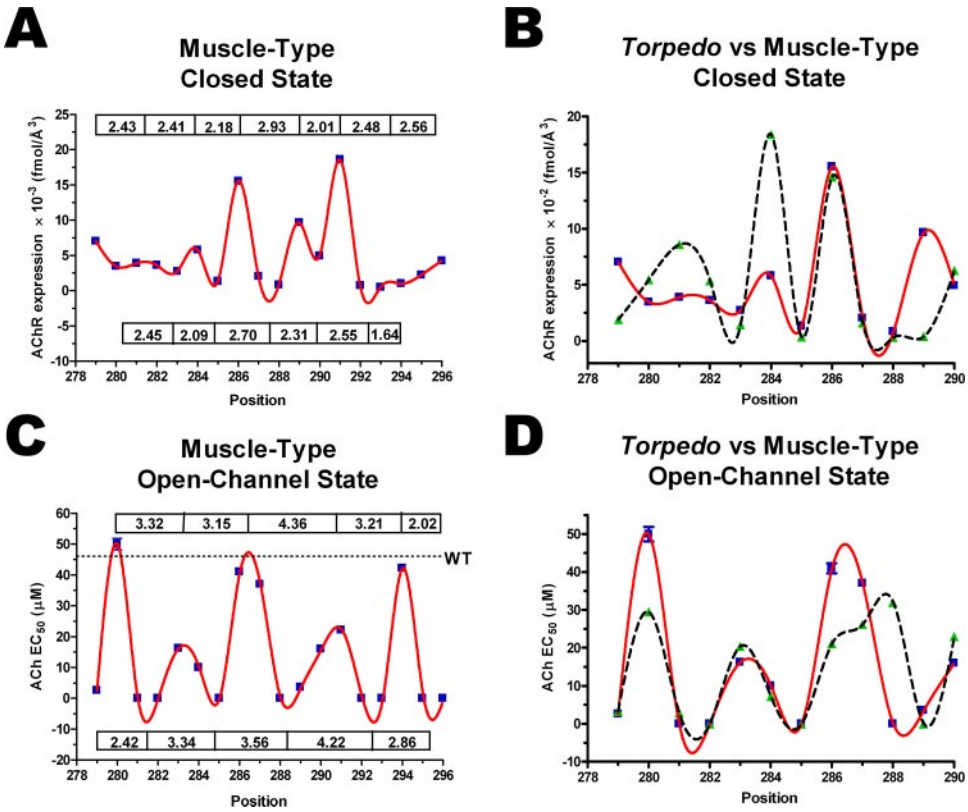

FIGURE 2. **Periodicity profiles of AChR expression and ACh EC_{50} of the *Torpedo* and muscle-type AChRs.** *A* and *C* show the periodicity profiles of the muscle-type AChR αM3 domain (*red line*) in the closed- (*A*) and open-channel (*C*) states. The values *inside* the *boxes* indicate the number of residues per helical turn between the adjacent maximums and minimums peaks. *B* and *D* illustrate the different oscillatory patterns of the *Torpedo* (*black dashed line*) and muscle-type (*red line*) AChRs in the closed- and open-channel states. *B* displays the muscle-type AChR plot with a magnification factor of 10 times (×10).

response, except F284W, which displayed a response similar to WT. Although the normalized macroscopic response was increased by five mutations (F280W, F284W, I286W, A287W, and I290W), it was drastically decreased by V283W and I289W (Table 1). The remaining three mutations (L279W, I291W, and I294W) displayed a normalized macroscopic response analogous to WT. The potency to acetylcholine (as measured by EC_{50}) was enhanced by 6 mutations (L279W, V283W, F284W, I289W, I290W, and I291W) from 200 to 1500% compared with WT (Fig. 1*C*). The reduction in EC_{50} values could be due to changes in affinity and/or efficacy of acetylcholine. On the other hand, 4 other mutations (F280W, I286W, A287W, and I294W) exhibited similar potency as WT. The present data suggest that tryptophan substitutions at positions αLeu-279, αVal-283, and αIle-289 produce a negative allosteric modulation given that these three mutations exhibit a decrease in macroscopic currents response while displaying increased AChR expression levels and ACh potencies (Table 1). In contrast, mutations F284W, I287W, I290W, and I291W displayed a gain-of-function response; their EC_{50} values shifted to lower ACh concentrations, while the peak currents and/or the normalized responses were larger than WT. Interestingly, residues αPhe-284 and αIle-287 have been labeled as exposed to the membrane lipids (10); therefore, these residues are believed to be hydrophobic allosteric sites (25, 32).

Five mutations (F280W, F284W, I286W, A287W, and I290W) showed the highest normalized response with low (*i.e.* F280W) or normal AChR expression levels and typical sigmoidal AChR response (Fig. 1*D*), except I286W, which considerably increased the AChR expression level and the functional response (Table 1). Three of those mutations (F280W, I286W, and A287W) exhibited normal potency (ACh EC_{50} values) relative to WT; on the contrary, A287W and I290W displayed the lowest ACh EC_{50} values. Mutations with the same AChR expression level as WT showed both a lower (*i.e.* V283W) and a similar (*i.e.* S279W) macroscopic response relative to WT. The normalized response results of the αM3 mutations have demonstrated that the tryptophan effect on the ion channel function of the AChR seems to depend on the mutation itself rather than in the variation of the AChR expression levels (25, 34).

Structural Characterization of the αM3 Domain—The periodicity of AChR expression (fmol/$Å^3$) revealed structural information of the αM3 domain for the closed state given that oocytes are incubated in an excess of toxin (~2 × 10^7-fold) to assure that all AChR in the oocyte surface are completely blocked by the toxin (see "Experimental Procedures"). Moreover, after α-BgTx incubation, oocytes do not display ACh-induced currents at any concentration of the agonist; thus, this is a clear indication that under these conditions all of the AChRs on the oocyte surface are bound with ^{125}I-labeled α-BgTx. In contrast, the periodicity profile from ACh EC_{50} (μM) values revealed structural information of the αM3 domain for the open-channel state given that the EC_{50} value estimates the functional state of the AChR. The periodicity profile of the closed state showed an ordered oscillation at the middle and rather disordered oscillation near its terminals, whereas the periodicity profile of the open-channel state displayed an ordered oscillation along all positions of the αM3 domain (Fig. 2, *A* and *C*). The ordered oscillatory pattern observed at the center of the closed state (*i.e.* positions αVal-285 through αIle-289) is consistent with a 3_{10} helical motif (61). Similar oscillatory patterns of 3_{10} helical structures containing 3–6 amino acids have been found in membrane-spanning domains of several membrane protein structures such as complex (oxireductase/antibody) (62, 63), hydrolase (64, 65), lipid transporter (66), mechanosensitive channel (67), membrane protein (68), oxidoreductase (69), oxireductase (70, 71), photosynthesis protein (72), signaling protein (73–77), and transport protein (78). The irregular oscillatory pattern presented at the ends of the

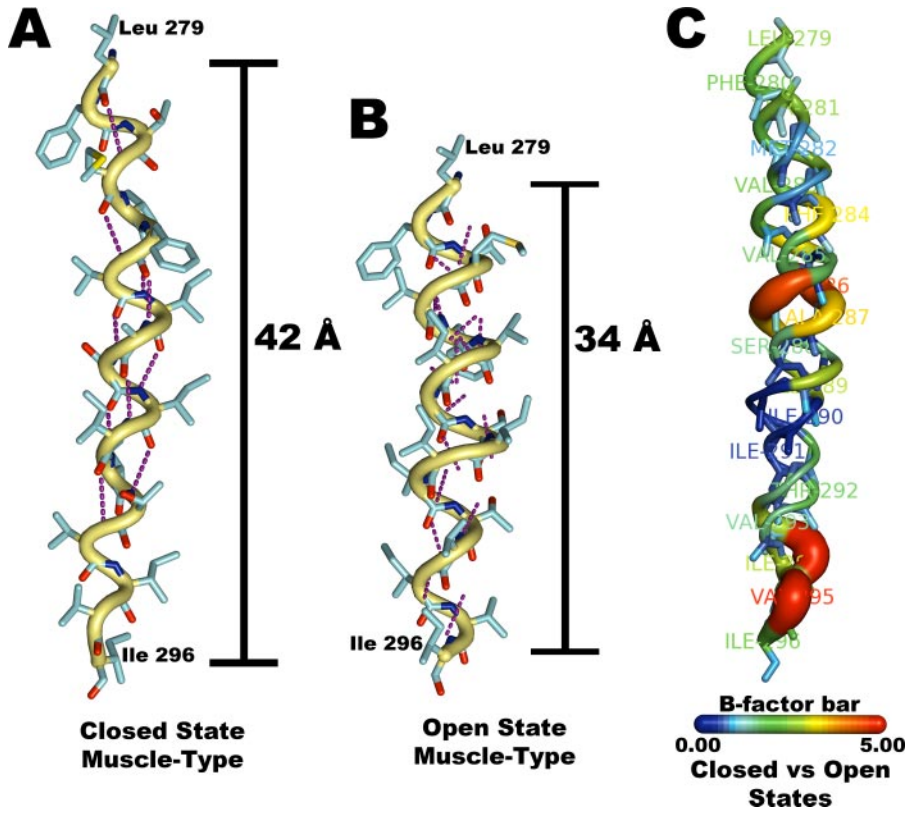

FIGURE 3. **αM3 structural models of the muscle-type AChR.** *A* and *B* show the helical structure of the αM3 domain in the closed- (*A*) and open-channel (*B*) states using the data of the periodicity profiles of the closed- and open-channel states, respectively (see Fig. 2, *A* and *C*). *Purple dashed dots* represent hydrogen bonds. *C* shows the B-factor of the superposition between αM3 models. The B-factor is an atomic displacement parameter that reflects the degree of mobility of an atom in the protein structure (82). The colors and thickness emphasize the conformational change of the backbone atoms in the superposed helical structures of the αM3 models. The root mean square deviation of the fit was 3.307 Å in 72 atoms. The root mean square deviation parameter estimates the quality of the fit between two superposed protein structures.

periodicity profile for the closed state suggests a disorganized helical structure of the αM3 domain. These findings agree with the NMR model of the αM3 peptide from *Torpedo* AChR that presented fewer constraints in both termini of the helical structure (79). It is noteworthy that the NMR model of the αM3 peptide might not necessary reflect the structure of the αM3 domain in the native receptor. The periodicity profiles of the αM3 domain in the closed- and open-channel states illustrate oscillatory patterns of 2.36 ± 0.33 and 3.25 ± 0.72 amino acids per helical turn, respectively, revealing a thinner-elongated helical structure for the closed state and a thicker-shrunken helical structure for the open-channel state (Figs. 2, *A* and *C*, and 3, *A* and *B*). The difference in oscillation patterns between the periodicity profiles of the closed- and open-channel states was observed to be about ~1.0 amino acid per helical turn, indicating a substantial conformational change (p value = 0.0041) along the αM3 domain as a consequence of channel activation of the AChR (Fig. 3*C*). The observed structural alteration could potentially affect the formation patterns of internal hydrogen bonds, the structural stabilization of the helix, the lipid-protein interactions, and/or the structural constraints with other transmembrane domains (Fig. 3, *A* and *B*). Similarly, the different sizes of helical structures of the αM3 domain for the closed- and open-channel states suggest that the helical structure displays a spring motion between the different conformational states of the muscle-type AChR. In addition, the helical net diagrams built with the periodicity profile data of the open-channel state (Fig. 2*C*) localize the αM3 mutants that produced gain-of-function and non-functional AChRs in different ranges of rotation angle (Fig. 4, *A* and *C*). The αM3 mutants that produced non-functional AChRs display an oscillation of ~3.5 residues/turn in the periodicity profile (Fig. 2*C*), are confined within a range of 180° (rotation angle) in the helical net diagrams (Fig. 4, *A* and *C*), and are clustered in the same face of the "open-channel state model" (Fig. 4, *B* and *D*). Together these data indicate that the αM3 domain preserves a helical secondary structure in the open-channel state. An apparent outlier is I289W, which is found in the region where all the non-functional AChRs are clustered; however, this mutant exhibits one of the lowest macroscopic peak currents. The fact that all the non-functional mutants are oriented toward the same face of the helix suggests a higher degree of packing within this region of the helix, presumably toward the interior of the protein. It is noteworthy that αLeu-279 and αIle-296, which are localized at the extremes of the periodicity profile of the open-channel state, cannot be taken as real minimum and maximum oscillatory peaks, respectively (Fig. 2*C*). As a consequence, in the helical net diagrams, the last helical turn of the maximum oscillatory peaks diagram (*upper segment*, Fig. 4*A*) and the first helical turn of the minimum oscillatory peaks diagram (*lower segment*, Fig. 4*C*) does not represent an accurate location of the gain-of-function and non-functional mutants, respectively. This particular observation shows the limitation of the helical net diagram analysis at the extremes of the helix, where it is very difficult to extrapolate a maximum and/or minimum oscillatory peak.

Structural Differences between the Torpedo and Muscle-type αM3 Domains—In the study by Guzman *et al.* (32) there are not enough amino acid positions in the C terminus side of the *Torpedo* AChR αM3 domain to allow for a complete comparison with the muscle-type AChR. However, we compared the αM3 domains from αLeu-279 through αIle-290, which include the N terminus and a large fraction at center of the helix. The closed state profiles for both AChR species displayed similar harmonized oscillatory patterns at residues αVal-283 through αAla-287 (Fig. 2*B*). In contrast, in the region of the N terminus and at residues αSer-288 through αIle-290, the oscillatory patterns are markedly different in both AChR species (Fig. 2*B*), suggesting that these two AChR species have different space requirements

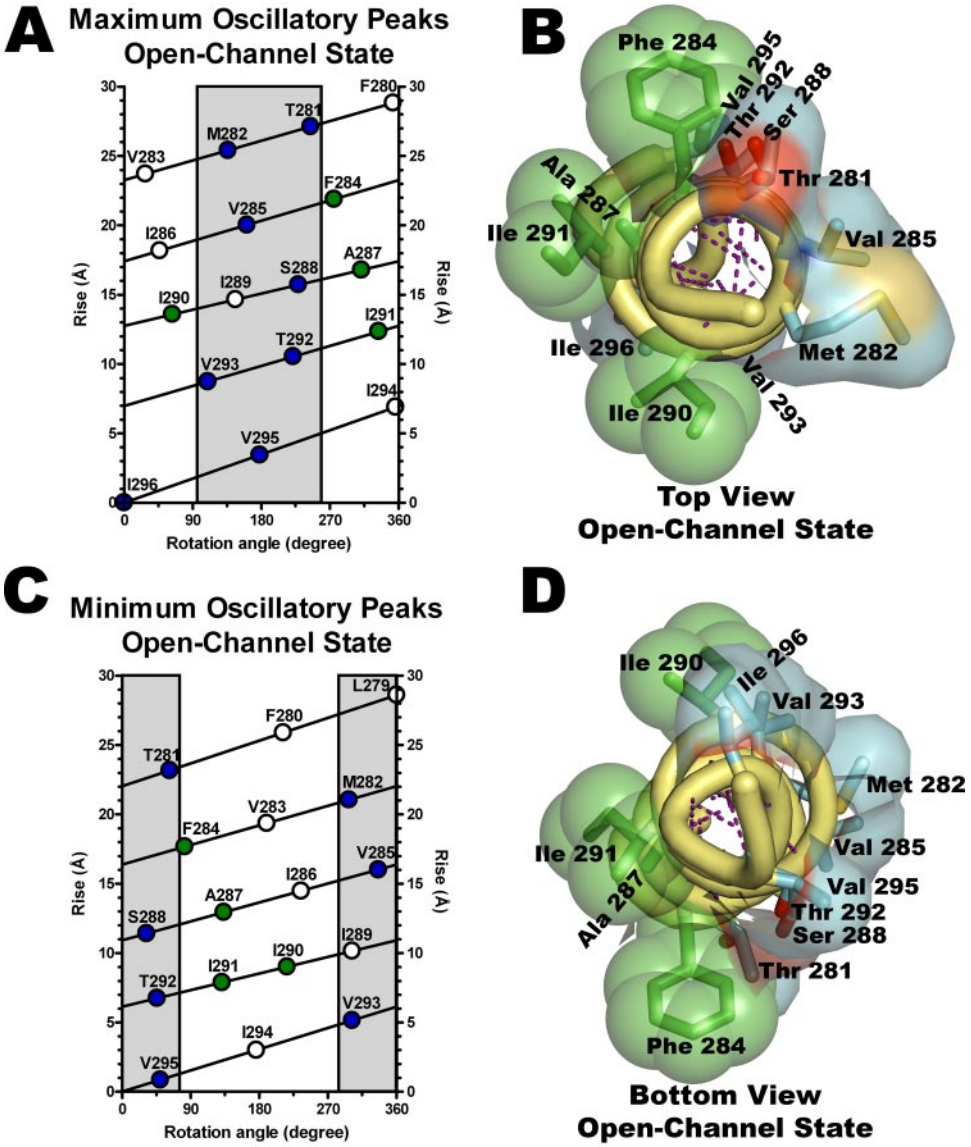

FIGURE 4. **Localization of the αM3-mutants of the muscle-type AChR in the open-channel state.** *A* and *C* exhibit the helical net diagrams of the amount of amino acids per helical turn between the adjacent maximum (*A*) and minimum (*C*) oscillatory peaks of the periodicity profile of the muscle-type AChR αM3 domain in the open-channel state (see Fig. 2*C*). The *gray box* delimits the area of the αM3-mutants that produced non-functional (*blue circle*) and gain-of-function (*green circle*) AChRs using the data of the open-channel state profile (see Fig. 2*C*). *B* and *D* display the αM3 mutants that produced non-functional (*cyan stick with surface side chains*) and gain-of-function (*green stick with sphere side chains*) AChRs using the open-channel state model (see Fig. 3*B*).

at these regions. The open-channel state profiles showed synchronized oscillatory patterns with a prominent shift at the lower half region, from αVal-285 to αIle-289 (Fig. 2*D*). In this region, the *Torpedo* AChR displayed a larger periodicity (4.39 residues per helical turn) than the muscle-type AChR (3.56 residues per helical turn), suggesting that *Torpedo* has a wider helical turn than muscle-type in the open-channel state. In addition, *Torpedo* AChR also present an additional hydroxyl group from the αSer-287 residue, which could generate a different pattern of hydrogen bond in this region (Fig. 1*A*).

DISCUSSION

In previous studies we have demonstrated that the tryptophan residue, the biggest amino acid, can be inserted along the αM3, αM4, βM3, γM3, and γM4 lipid-exposed domains of the AChR (25, 27, 32–35). Here, we provide both functional and structural interpretations for the αM3 Trp-ScanM in correlation with previous TrpScanM studies, photolabeling affinity studies (10, 12), and the most recent *T. marmorata* AChR structure (6). In addition, we examine the functional and structural differences between the αM3 domains of the *Torpedo* and muscle-type receptors AChR.

Functional Interpretation of the αM3 Tryptophan Scanning—In contrast to our previous studies (25, 27, 32–35), we have found 6 mutations (αF280W, αV285W, αS288W, αT292W, αV293W, and αI294W) that produce significant reductions in the AChR expression levels, suggesting a reduced efficiency of assembly and/or oligomerization of the AChR. Previously, 3-trifluoromethyl-3-(*m*-[^{125}I]iodophenyl)diazirine) photolabeling studies in the *Torpedo californica* AChR suggested that these residues are oriented toward the AChR interior, away from the lipid membrane (10). Consistent with the study performed in the *T. californica* AChR αM3 domain (32), the mutations αF280W, αV285W, and αS288W also displayed dramatic reductions in the AChR expression levels, suggesting that these positions are critical to the AChR assembly and/or oligomerization.

The high number of mutations that resulted in non-functional AChRs (ND in Table 1) suggests that the αM3 domain is more tightly packed toward the AChR interior than our previous TrpScanM studies (25, 32, 34, 35). According to the cryoelectron microscopic data, the high density of non-functional mutations from αThr-292 to αIle-296 residues is expected due to a highly constricted space among all the AChR transmembrane domains near the cytoplasmic side (6). Of the eight non-functional mutations, four mutations (αV285W, αS288W, αT292W, and αV293W) displayed very low AChR expression levels, which could lead to the observed loss of ion channel function of the AChR. Three of these mutations (αV285W, αS288W, and αT292W) are localized at positions that have been previously proposed to form two extremely stable internal hydrogen bonds; therefore, we suggest that the disruption of these bonds could lead to destabilization of the helical structure and the

functional dynamics of the αM3 domain (79). The loss of ion channel function of the remaining four mutations (αT281W, αM282W, αV295W, and αI296W) that displayed similar AChR expression levels as WT could be due to intra- and/or inter-transmembrane interactions that stabilize the open-channel state of the AChR. Also, the non-functionality of two of these mutations (αM282W and αV285W) agree with the previous αM3 *Torpedo* study (32), thus suggesting that αMet-282 and αVal-285 are critical constraint positions in both AChR species. Furthermore, previous mutations at the αVal-285 position revealed that changes in stereochemistry and volume at this site affect the ion channel function of the AChR (23, 32, 33).

We have previously demonstrated that a single tryptophan substitution in the lipid-exposed domains can enhance the ion channel function of the AChR (17–21, 24, 25, 27, 32–35). In contrast, the introduction of the tryptophan residue significantly reduced the macroscopic response in five mutations (αL279W, αF280W, αV283W, αI289W, and αI294W), suggesting an impaired ion channel function of the AChR. Moreover, αL279W, αV283W, and αI289W resulted in a significant inhibition of the ion channel function, producing sufficient AChR expression levels; therefore, the reduced peak currents were very likely due to the lock up of AChRs in a dysfunctional conformation. Another possible explanation is that the fraction of these mutated receptors in the resting conformation was significantly reduced compared with WT. On the other hand, αF280W and αI294W showed a significant decrease in the peak currents and in the AChR expression levels, which suggests a decrease in the efficiency of assembly and/or oligomerization of the receptor.

The increase in the macroscopic response of four mutations (αI286W, αA287W, αI290W, and αI291W) suggests an enhancement in the modulation and/or ion channel properties of the AChR. In a previous study αS287W and αI290W were also identified as gain-of-function mutations in the muscle-type AChR (33). The enhancement of ion channel function by αI286W and αI291W could be related to the observed increase in the AChR expression levels despite having different ACh EC_{50} values and normalized responses. Overall, the functional data of the αM3 mutations have demonstrated that the αM3 domain plays a pivotal role in the ion channel gating of the muscle-type AChR.

Structural Interpretation of the αM3 Domain; Closed- Versus Open-channel States—In the present study the tryptophan periodicity profiles of the αM3 domain display distinctive structural differences between the closed- and open-channel states of the muscle-type AChR. These profiles indicate two different helical structures; a thinner-elongated helix for the closed state (Fig. 3*A*) and a thicker-shrunken helix for the open-channel state (Fig. 3*B*). The number of amino acids per helical turn of the tryptophan periodicity profiles served as a template to build the "closed-" and "open-channel state" models (Figs. 2, *A* and *C*, and 3, *A* and *B*). The superimposition of the closed- and open-channel state models provided information of the conformational change of the αM3 domain during channel activation of the AChR. The comparison between the structural models revealed the conformational changes undergone by the αM3 domain, emphasized in colors and thickness (Fig. 3*C*). The αM3 superimposition model displays moderate conformational changes (helical thickness) along the αM3 domain of the muscle-type AChR. These localized conformational changes could be a consequence of the number of internal hydrogen bonds that are broken and/or formed in the helical structure (Fig. 3, *A–C*). Also, the colors in the αM3 superimposition model suggest a disorganized pattern of structural displacements between the closed- and open-channel αM3 conformations (Fig. 3*C*). In addition, the open-channel state model presented a 20% larger volume than the closed state model, suggesting structural displacements by the αM3 domain in the open-channel state of the AChR (Fig. 3, *A* and *B*). Therefore, the expansion of the αM3 helical structure will further increase the structural constrain at the membrane-spanning region of the AChR in the open-channel state. The open state-channel model also shows that all the "non-functional" and gain-of-function residues are clustered in opposite sides of the helix; however, the non-functional positions cover ~50% of the circumference surface of the helical structure (Figs. 4, *A–D*). These findings suggest that the movement of the bulky tryptophan side chain at these positions during gating transitions of the AChR will affect key helix-helix contacts; thus, the present model built from periodicity profile data is consistent with the functional data gathered from the TrpScanM approach.

Comparison between Torpedo and Muscle-type αM3 Domains—Although the αM3 domain is the most conserved among lipid-exposed transmembrane domains, a homology sequence alignment of the αM3 domains showed three residues (αVal-283, αAla-287, and αIle-294) that are not conserved between *Torpedo* and muscle-type AChRs (Fig. 1*A*). Also, we previously found functional divergence between these receptors at positions αPhe-284, αAla-287, and αIle-290 (32, 33). In the present study the prominent periodicity shift in the periodicity profile of the open-channel state that occurs from positions αVal-285 to αIle-289 is consistent with these functional divergences (Fig. 2*D*). Moreover, the S288W mutant in the *Torpedo* receptor displayed a reduced functional response, whereas for the muscle-type receptor it leads to a non-functional AChR (Table 1). However, the I289W mutant in the muscle-type receptor led to a reduced functional response, whereas the same mutation in the *Torpedo* receptor produced a non-functional AChR (32). We suggest that at this particular region there could be differences in helical packing, pattern of internal hydrogen bonds, and/or stability of the helical structure (conformational rigidity) in the open-channel state that could contribute to divergence in the ion channel function of both AChR species.

Concluding Remarks—The present αM3 TrpScanM demonstrates that the αM3 domain plays a pivotal role in the ion channel gating of the muscle-type AChR. These results support the notion that the αM3 domain undergoes a spring motion during ion channel activation indicating a significant conformational change. There are remarkable functional and structural differences between the αM3 muscle type and the *Torpedo* AChR (32, 33). We suggest that some of the localized structural differences in the αM3 between these two receptors could contribute to these functional differences.

One hypothetical model that could be considered based on the present results is that the helical structure in the closed state could be tilted with respect to the membrane bilayer and/or to its actual position in the open-channel state. The main argument to support this hypothetical model is based on the estimated length of the helix, which suggests an expansion in the *z* axis of ~8–10 Å in the closed state. The longitudinal expansion in the *z* axis predicts that the helix within a lipid bilayer of constant thickness (80) could be tilted to minimize the exposition of the terminal hydrophobic amino acid residues into an aqueous environment. This hypothetical model is supported by two independent studies. First, in the positive hydrophobic mismatch condition, *i.e.* a protein hydrophobic length that is greater than the thickness of the lipid hydrophobic region, simulated of transmembrane peptides in lipid bilayers, can adopt various tilt angles to reduce the exposure to polar environment (81). Second, the highest number of incorporation sites by a photoactivable hydrophobic probe, 3-trifluoromethyl-3-(*m*-[^{125}I]iodophenyl)diazirine, into the lipid-exposed domains of the AChR in the absence of carbamylcholine (agonist analogue) indicates that the surface of the lipid-AChR interface in the resting state is larger than in the desensitized state (12). These 3-trifluoromethyl-3-(*m*-[^{125}I]iodophenyl)diazirine-labeling data are consistent with the tilted helix in the closed state given that the αM3 domain has a greater longitudinal surface area to make contact with the membrane lipids (12).

Our long-term goal is to extend the same analysis to the entire lipid-exposed transmembrane domains (*i.e.* M3 and M4) of the AChR to test the proposed model of a spring motion in the αM3 domain. A detailed analysis of these domains will provide information to establish potential differences in spatial orientation, allosteric sites, constraint sites, and helical patterns of each domain in the closed- and open-channel states. Nevertheless, from the previous TrpScanM studies (25, 32, 34, 35), it seems evident that this αM3 domain has a unique pattern that is consistent with a spring motion. The proposed spring model suggested in the present study represents a framework for comparative studies with other ligand-gated ion channel receptors. Ultimately, decoding the complex network of lipid-protein interactions may lead to an understanding of the dynamics of conformational transitions of membrane proteins.

Acknowledgments—We especially thank José E. Lizardi, Eric Velázquez, Fernando X. Cuascut, Noelis M. Rosario, and Carla P. Rodríguez for excellent technical assistance.

REFERENCES

1. Karlin, A. (2002) *Nat. Rev. Neurosci.* **3,** 102–114
2. Corringer, P. J., Le Novere, N., and Changeux, J. P. (2000) *Annu. Rev. Pharmacol. Toxicol.* **40,** 431–458
3. Le Novere, N., Corringer, P. J., and Changeux, J. P. (2002) *J. Neurobiol.* **53,** 447–456
4. Cockcroft, V. B., Osguthorpe, D. J., Barnard, E. A., Friday, A. E., and Lunt, G. G. (1990) *Mol. Neurobiol.* **4,** 129–169
5. Engel, A. G., Ohno, K., and Sine, S. M. (2002) *Mol. Neurobiol.* **26,** 347–367
6. Unwin, N. (2005) *J. Mol. Biol.* **346,** 967–989
7. Devillers-Thiery, A., Galzi, J. L., Eisele, J. L., Bertrand, S., Bertrand, D., and Changeux, J. P. (1993) *J. Membr. Biol.* **136,** 97–112
8. Unwin, N. (1995) *Nature* **373,** 37–43
9. Miyazawa, A., Fujiyoshi, Y., and Unwin, N. (2003) *Nature* **423,** 949–955
10. Blanton, M. P., and Cohen, J. B. (1994) *Biochemistry* **33,** 2859–2872
11. Wilson, G., and Karlin, A. (2001) *Proc. Natl. Acad. Sci. U. S. A.* **98,** 1241–1248
12. daCosta, C. J., Ogrel, A. A., McCardy, E. A., Blanton, M. P., and Baenziger, J. E. (2002) *J. Biol. Chem.* **277,** 201–208
13. Leite, J. F., Blanton, M. P., Shahgholi, M., Dougherty, D. A., and Lester, H. A. (2003) *Proc. Natl. Acad. Sci. U. S. A.* **100,** 13054–13059
14. Cymes, G. D., Ni, Y., and Grosman, C. (2005) *Nature* **438,** 975–980
15. Wang, H. L., Auerbach, A., Bren, N., Ohno, K., Engel, A. G., and Sine, S. M. (1997) *J. Gen. Physiol.* **109,** 757–766
16. Cymes, G. D., Grosman, C., and Auerbach, A. (2002) *Biochemistry* **41,** 5548–5555
17. Li, L., Schuchard, M., Palma, A., Pradier, L., and McNamee, M. G. (1990) *Biochemistry* **29,** 5428–5436
18. Li, L., Lee, Y. H., Pappone, P., Palma, A., and McNamee, M. G. (1992) *Biophys. J.* **62,** 61–63
19. Lee, Y. H., Li, L., Lasalde, J., Rojas, L., McNamee, M., Ortiz-Miranda, S. I., and Pappone, P. (1994) *Biophys. J.* **66,** 646–653
20. Lasalde, J. A., Tamamizu, S., Butler, D. H., Vibat, C. R., Hung, B., and McNamee, M. G. (1996) *Biochemistry* **35,** 14139–14148
21. Ortiz-Miranda, S. I., Lasalde, J. A., Pappone, P. A., and McNamee, M. G. (1997) *J. Membr. Biol.* **158,** 17–30
22. Campos-Caro, A., Rovira, J. C., Vicente-Agullo, F., Ballesta, J. J., Sala, S., Criado, M., and Sala, F. (1997) *Biochemistry* **36,** 2709–2715
23. Wang, H. L., Milone, M., Ohno, K., Shen, X. M., Tsujino, A., Batocchi, A. P., Tonali, P., Brengman, J., Engel, A. G., and Sine, S. M. (1999) *Nat. Neurosci.* **2,** 226–233
24. Tamamizu, S., Lee, Y., Hung, B., McNamee, M. G., and Lasalde-Dominicci, J. A. (1999) *J. Membr. Biol.* **170,** 157–164
25. Tamamizu, S., Guzman, G. R., Santiago, J., Rojas, L. V., McNamee, M. G., and Lasalde-Dominicci, J. A. (2000) *Biochemistry* **39,** 4666–4673
26. Bouzat, C., Barrantes, F., and Sine, S. (2000) *J. Gen. Physiol.* **115,** 663–672
27. Cruz-Martin, A., Mercado, J. L., Rojas, L. V., McNamee, M. G., and Lasalde-Dominicci, J. A. (2001) *J. Membr. Biol.* **183,** 61–70
28. Santiago, J., Guzman, G. R., Rojas, L. V., Marti, R., Asmar-Rovira, G. A., Santana, L. F., McNamee, M., and Lasalde-Dominicci, J. A. (2001) *J. Biol. Chem.* **276,** 46523–46532
29. Bouzat, C., Gumilar, F., del Carmen Esandi, M., and Sine, S. M. (2002) *Biophys. J.* **82,** 1920–1929
30. Garbus, I., Roccamo, A. M., and Barrantes, F. J. (2002) *Neuropharmacology* **43,** 65–73
31. De Rosa, M. J., Rayes, D., Spitzmaul, G., and Bouzat, C. (2002) *Mol. Pharmacol.* **62,** 406–414
32. Guzman, G. R., Santiago, J., Ricardo, A., Marti-Arbona, R., Rojas, L. V., and Lasalde-Dominicci, J. A. (2003) *Biochemistry* **42,** 12243–12250
33. Navedo, M., Nieves, M., Rojas, L., and Lasalde-Dominicci, J. A. (2004) *Biochemistry* **43,** 78–84
34. Santiago, J., Guzman, G. R., Torruellas, K., Rojas, L. V., and Lasalde-Dominicci, J. A. (2004) *Biochemistry* **43,** 10064–10070
35. Ortiz-Acevedo, A., Melendez, M., Asseo, A. M., Biaggi, N., Rojas, L. V., and Lasalde-Dominicci, J. A. (2004) *J. Biol. Chem.* **279,** 42250–42257
36. Mitra, A., Bailey, T. D., and Auerbach, A. L. (2004) *Structure* (*Camb*) **12,** 1909–1918
37. Shen, X. M., Deymeer, F., Sine, S. M., and Engel, A. G. (2006) *Ann. Neurol.* **60,** 128–136
38. Blanton, M. P., Dangott, L. J., Raja, S. K., Lala, A. K., and Cohen, J. B. (1998) *J. Biol. Chem.* **273,** 8659–8668
39. Blanton, M. P., McCardy, E. A., Huggins, A., and Parikh, D. (1998) *Biochemistry* **37,** 14545–14555
40. Jung, S., Akabas, M. H., and Harris, R. A. (2005) *J. Biol. Chem.* **280,** 308–316
41. Choe, S., Stevens, C. F., and Sullivan, J. M. (1995) *Proc. Natl. Acad. Sci. U. S. A.* **92,** 12046–12049
42. Collins, A., Chuang, H., Jan, Y. N., and Jan, L. Y. (1997) *Proc. Natl. Acad. Sci. U. S. A.* **94,** 5456–5460
43. Cukras, C. A., Jeliazkova, I., and Nichols, C. G. (2002) *J. Gen. Physiol.* **119,** 581–591

44. Monks, S. A., Needleman, D. J., and Miller, C. (1999) *J. Gen. Physiol.* **113,** 415–423
45. Hong, K. H., and Miller, C. (2000) *J. Gen. Physiol.* **115,** 51–58
46. Li-Smerin, Y., Hackos, D. H., and Swartz, K. J. (2000) *Neuron* **25,** 411–423
47. Li-Smerin, Y., Hackos, D. H., and Swartz, K. J. (2000) *J. Gen. Physiol.* **115,** 33–50
48. Li-Smerin, Y., and Swartz, K. J. (2001) *J. Gen. Physiol.* **117,** 205–218
49. Hackos, D. H., Chang, T. H., and Swartz, K. J. (2002) *J. Gen. Physiol.* **119,** 521–532
50. Irizarry, S. N., Kutluay, E., Drews, G., Hart, S. J., and Heginbotham, L. (2002) *Biochemistry* **41,** 13653–13662
51. Panchenko, V. A., Glasser, C. R., and Mayer, M. L. (2001) *J. Gen. Physiol.* **117,** 345–360
52. Ueno, S., Lin, A., Nikolaeva, N., Trudell, J. R., Mihic, S. J., Harris, R. A., and Harrison, N. L. (2000) *Br. J. Pharmacol.* **131,** 296–302
53. Jenkins, A., Andreasen, A., Trudell, J. R., and Harrison, N. L. (2002) *Neuropharmacology* **43,** 669–678
54. Wang, S. Y., Bonner, K., Russell, C., and Wang, G. K. (2003) *Biophys. J.* **85,** 911–920
55. Honse, Y., Ren, H., Lipsky, R. H., and Peoples, R. W. (2004) *Neuropharmacology* **46,** 647–654
56. Silberberg, S. D., Chang, T. H., and Swartz, K. J. (2005) *J. Gen. Physiol.* **125,** 347–359
57. Powl, A. M., Wright, J. N., East, J. M., and Lee, A. G. (2005) *Biochemistry* **44,** 5713–5721
58. Subbiah, R. N., Kondo, M., Campbell, T. J., and Vandenberg, J. I. (2005) *J. Physiol.* (*Lond.*) **569,** 367–379
59. Kashlan, O. B., Maarouf, A. B., Kussius, C., Denshaw, R. M., Blumenthal, K. M., and Kleyman, T. R. (2006) *J. Biol. Chem.* **281,** 30455–30462
60. Chothia, C. (1975) *Nature* **254,** 304–308
61. Iwata, T., Lee, S., Oishi, O., Aoyagi, H., Ohno, M., Anzai, K., Kirino, Y., and Sugihara, G. (1994) *J. Biol. Chem.* **269,** 4928–4933
62. Ostermeier, C., Harrenga, A., Ermler, U., and Michel, H. (1997) *Proc. Natl. Acad. Sci. U. S. A.* **94,** 10547–10553
63. Harrenga, A., and Michel, H. (1999) *J. Biol. Chem.* **274,** 33296–33299
64. Toyoshima, C., Nakasako, M., Nomura, H., and Ogawa, H. (2000) *Nature* **405,** 647–655
65. Sorensen, T. L., Moller, J. V., and Nissen, P. (2004) *Science* **304,** 1672–1675
66. Chang, G. (2003) *J. Mol. Biol.* **330,** 419–430
67. Chang, G., Spencer, R. H., Lee, A. T., Barclay, M. T., and Rees, D. C. (1998) *Science* **282,** 2220–2226
68. Ren, G., Reddy, V. S., Cheng, A., Melnyk, P., and Mitra, A. K. (2001) *Proc. Natl. Acad. Sci. U. S. A.* **98,** 1398–1403
69. Soulimane, T., Buse, G., Bourenkov, G. P., Bartunik, H. D., Huber, R., and Than, M. E. (2000) *EMBO J.* **19,** 1766–1776
70. Lancaster, C. R., Kroger, A., Auer, M., and Michel, H. (1999) *Nature* **402,** 377–385
71. Lancaster, C. R., Gross, R., and Simon, J. (2001) *Eur. J. Biochem.* **268,** 1820–1827
72. Liu, Z., Yan, H., Wang, K., Kuang, T., Zhang, J., Gui, L., An, X., and Chang, W. (2004) *Nature* **428,** 287–292
73. Palczewski, K., Kumasaka, T., Hori, T., Behnke, C. A., Motoshima, H., Fox, B. A., Le Trong, I., Teller, D. C., Okada, T., Stenkamp, R. E., Yamamoto, M., and Miyano, M. (2000) *Science* **289,** 739–745
74. Teller, D. C., Okada, T., Behnke, C. A., Palczewski, K., and Stenkamp, R. E. (2001) *Biochemistry* **40,** 7761–7772
75. Okada, T., Fujiyoshi, Y., Silow, M., Navarro, J., Landau, E. M., and Shichida, Y. (2002) *Proc. Natl. Acad. Sci. U. S. A.* **99,** 5982–5987
76. Okada, T., Sugihara, M., Bondar, A. N., Elstner, M., Entel, P., and Buss, V. (2004) *J. Mol. Biol.* **342,** 571–583
77. Li, J., Edwards, P. C., Burghammer, M., Villa, C., and Schertler, G. F. (2004) *J. Mol. Biol.* **343,** 1409–1438
78. Abramson, J., Smirnova, I., Kasho, V., Verner, G., Kaback, H. R., and Iwata, S. (2003) *Science* **301,** 610–615
79. Lugovskoy, A. A., Maslennikov, I. V., Utkin, Y. N., Tsetlin, V. I., Cohen, J. B., and Arseniev, A. S. (1998) *Eur. J. Biochem.* **255,** 455–461
80. McIntosh, T. J., and Simon, S. A. (1986) *Biochemistry* **25,** 4058–4066
81. Kandasamy, S. K., and Larson, R. G. (2006) *Biophys. J.* **90,** 2326–2343
82. Smith, D. K., Radivojac, P., Obradovic, Z., Dunker, A. K., and Zhu, G. (2003) *Protein Sci.* **12,** 1060–1072